Three-Legged 2,2′-Bipyridine Monomer at the Air/Water Interface: Monolayer Structure and Reactions with Ni(II) Ions from the Subphase

Wenyang Dai,[†] Lay-Theng Lee,[‡] Andri Schütz,[†] Benjamin Zelenay,[†] Zhikun Zheng,[†] Andreas Borgschulte,[§] Max Döbeli,[‖] Wasim Abuillan,[⊥] Oleg V. Konovalov,[#] Motomu Tanaka,*[,⊥,∇] and A. Dieter Schlüter*[,†]

[†]Laboratory of Polymer Chemistry, Department of Materials, ETH Zurich, Vladimir-Prelog-Weg 5, 8093 Zürich, Switzerland

[‡]Laboratoire Léon Brillouin, CEA-CNRS, Université Paris-Saclay, CEA-Saclay, 91191 Gif-sur-Yvette Cedex, France

[§]Empa, Swiss Federal Laboratories for Materials Science and Technology, Advanced Analytical Technologies, Überlandstrasse 129, 8600 Dübendorf, Switzerland

[‖]Ion Beam Physics HPK H32, ETH Zurich, Otto-Stern-Weg 5, 8093 Zurich, Switzerland

[⊥]Physical Chemistry of Biosystems, Institute of Physical Chemistry, University of Heidelberg, 69120 Heidelberg, Germany

[#]European Synchrotron Radiation Facility (ESRF), CS 40220, 38043 Grenoble Cedex 9, France

[∇]Institute for Integrated Cell-Material Sciences (iCeMS), Kyoto University, Kyoto 606-8501, Japan

S *Supporting Information*

ABSTRACT: The behavior of compound **2** [1,3,5-tri(2,2′-bipyridin-5-yl)benzene] with three bipyridine units arranged in a star geometry is investigated in the presence and absence of $Ni(ClO_4)_2$. Its properties at the air−water interface as well as after transfer onto a solid substrate are studied by several techniques including Brewster angle microscopy, X-ray reflectivity, neutron reflectivity, X-ray photoelectron spectroscopy, Rutherford backscattering spectrometry, and atomic force microscopy combined with optical microscopy. It is found that compound **2** within the monolayers formed stays almost vertical at the interface and that at high $Ni^{2+}/2$ ($Ni^{2+}/2$ = 4000, 20′000) ratios two of the three bipyridine units of **2** are complexed, resulting in supramolecular sheets that are likely composed of arrays of linear metal−organic complexation polymers.

Top view on sheet
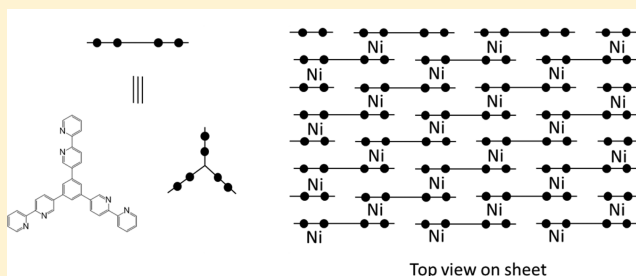
1. INTRODUCTION

Starting with the work by Gee et al. in 1936,[1,2] chemists have been interested in the creation of infinitely large monolayer (ML) sheets and whether they can be provided with long-range internal order (periodicity, crystallinity).[3] Mild methods to synthesize monolayer sheets with strong internal bonds are attractive because they in principle allow for rational structure design and the placement of functional groups on the sheets at predetermined sites.[4−10] We and others have therefore started to explore the accessibility of ML sheets including two-dimensional polymers (2DP) both in single crystals[11−14] and at the air/water interface.[15−20] Attempts in solution have also been reported.[21,22] Although the single-crystal approach has in fact led to the proven 2DPs, the air/water interface approach offers access to ML sheets with macroscopic size at the expense, however, of a more complex structure elucidation on the molecular level. Nevertheless, both metal−organic and covalent ML sheets exhibiting mechanical coherence and considerable mechanical stability were realized.[15−20]

Metal−organic sheets were obtained using terpyridine (tpy)-based monomers such as hexafunctional compound **1** (Figure 1). Metal cations Fe^{2+}, Co^{2+}, Ni^{2+}, and Zn^{2+} served as connectors and were provided from the subphase to the spread and compressed monomer ML lying flat at the air/water interface.[15,16] Within minutes to hours, mechanically stable sheets formed with $[Met(tpy)_2]^{2+}$ (Met = metal) complexes as the netpoints. Motivated by this particularly easy and mild access to robust and free-standing sheets, we started a program exploring other types of monomers for network formation and concentrated first on compounds that carry peripheral 4,4′-bipyridine (bpy) for possible metal complexation. Figure 1 shows the first studied example, trifunctional compound **2**. The choice of bpy as a ligand was in part motivated by the consideration that a square planar complexation of bpy units[23,24] at net points could have advantages over the
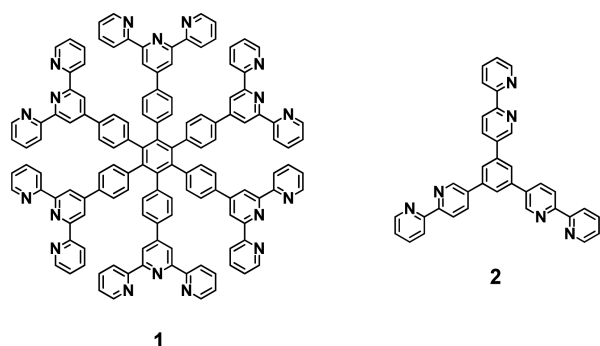
Figure 1. Chemical structures of monomers **1** and **2**. Monomer **1** carries six terpyridine units, and monomer **2** carries three bipyridine units intended to serve as ligands for metal ion complexation when spread at an air/water interface.

rectangular complexation typical for tpy's when analyzing the molecular structure by STM. At first, however, we were curious to see whether the novel bpy-based compounds would lie flat on the water surface or assume other arrangements that could open access to novel kinds of ML sheets complementing the now existing ones. In particular, porphyrin and phthalocyanine derivates often stand up on water, assuming different tilt angles to the surface normal,[25−29] though there are also exceptions.[30,31]

Here we describe the spreading behavior of **2** at the air/water interface into the corresponding monolayers **ML2** as observed by the surface pressure/mean molecular area (MMA) isotherms and by Brewster's angle microscopy (BAM). The **ML2** thickness is determined before transfer by X-ray reflectivity (XRR) and after transfer onto a solid substrate by AFM (Si/SiO$_2$) and neutron reflectivity (NR, Si wafer). Together with the MMA values, this led us to propose that compound **2** does not lie flat on the water surface. Next we describe the exposure of **ML2** to varying ratios of Ni(ClO$_4$)$_2$ to see whether a planar conformation of the monomers can be enforced through complexation or an alternative complexation mode is favored in which the vertically standing constituents are stitched together by complexation of the bpy units pointing downward. After this exposure, **ML2** is referred to as sheets, **S2$_{Ni}$**, whereby the subscript denotes the Ni^{2+}/**2**-ratio used for sheet synthesis. Finally, we report the results of X-ray reflectivity (XRR), neutron reflectivity (NR), Rutherford backscattering spectroscopy (RBS), and X-ray photoelectron spectroscopy (XPS) to arrive at an estimation of the stoichiometry between monomer **2** and Ni^{2+} in the sheets, **S2$_{Ni}$**. XPS is further used to prove whether the Ni^{2+} ions are actually complexed to the bpy units of **2** and to which degree this is the case for the different Ni^{2+}/**2** ratios applied. Despite the fact that the full characterization of MLs is experimentally challenging, the combination of these four experimental tools provides valuable insights into this stoichiometric structural information, which led us to propose a provisory model for **S2$_{Ni}$**.

2. MATERIALS AND METHODS

2.A. Monomer Synthesis and Monomer Size. The key compound for synthesis is bipyridine **3**, which was synthesized on the 5 g scale according to known Negishi coupling procedures.[32,33] Bromide **3** was directly coupled with 1,3,5-benzene trisboronic ester **4**[34] to monomer **2** using standard Suzuki Miyaura cross-coupling conditions (Figure 2). Monomer **2** was recrystallized from acetonitrile and obtained on the 100 mg scale. Its proton NMR spectrum showed a singlet for the aromatic protons of the central ring at δ = 7.95 ppm,
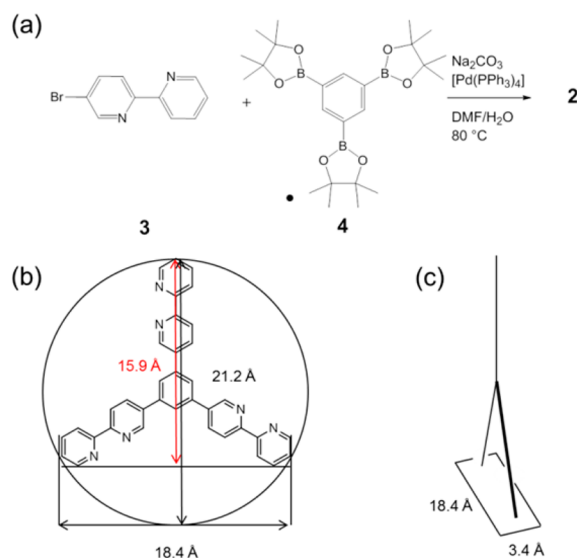

Figure 2. (a) Synthesis sequence to obtain monomer **2**. Estimation of the size of monomer **2** in Å: (b) top view and (c) simplified side view. The sizes include the relevant hydrogen atoms, which are not shown for clarity.

proving the symmetry. The size of monomer **2** was estimated by simple geometric considerations (Figure 2). Assuming the monomer to be a disc, the diameter D of this disc will be on the order of $D \approx 21$ Å, and the area A will be ~300 Å^2. Assuming the monomer to stand upright with two of its bpy units pointing downward, the height h will be ~16 Å and the projected area on the surface will be 18.4 × 3.4 Å^2 ≈ 63 Å^2, assuming a molecule thickness resembling that of graphene (3.4 Å).

2.B. Monolayer Formation and Exposure to Ni(ClO$_4$)$_2$. A dilute chloroform solution (0.5 mg/mL) of compound **2** was spread at an air/water interface, and the formation of monolayer **ML2** was observed with BAM. After an equilibration time of 30 min at 8 mN m^{-1}, **ML2** was exposed to concentrated Ni(ClO$_4$)$_2$ solutions (0.5−5 mL) that were injected into the subphase beneath the spread ML. The following ratios of total Ni(ClO$_4$)$_2$ in the subphase to monomer **2** at the interface were applied: Ni^{2+}/**2** = 400, 4000, and 20′000, resulting in sheets **S2$_{400}$**, **S2$_{4000}$**, and **S2$_{20′000}$**, respectively. Not for all measurements were these three Ni^{2+}/**2** ratios applied. To guarantee that the system reaches the saturation level of complexation, the exposure time was set to 15 h if not otherwise noted.

2.C. X-ray Reflectivity. XRR experiments were carried out at beamline ID10B of the European Synchrotron Radiation Facility (ESRF, Grenoble). The monolayers were irradiated with a monochromatic synchrotron beam with energy of 8 keV corresponding to a wavelength of λ = 1.55 Å. The XRR curves were recorded at angles of incidence of θ = 0 to 4.6°, giving a range of momentum transfer from 0 to 0.65 Å^{-1}. The reflectivity was normalized to the incident beam and analyzed using the Parratt formalism[35] with a genetic minimization algorithm implemented in the MOTOFIT software package.[36] The incident angle θ was transformed into the scattering vector component normal to the interface, $q_z = 4\pi \sin(\theta)/\lambda$.

2.D. Monolayer and Sheet Transfer. Monolayers **ML2** and Ni-exposed monolayers, sheets **S2$_{400−20′000}$**, were horizontally transferred onto various substrates depending on the intended analytical method used for characterization. As substrates, Si/SiO$_2$ (280 nm) for AFM and RBS, silicon wafers with an oxide layer of approximately 1 nm for NR, and Si/SiO$_2$ (280 nm) covered with an Au layer (200 nm) for XPS were used. The sheets were dried for 3 h after transfer under ambient conditions and investigated as obtained.

The sheet heights were determined (among other methods; see later) by tapping-mode AFM (TM-AFM) after transfer onto silicon wafers (Discussion section), whereby the necessary edges were created by removing a piece of mica that had been deposited on the substrate

prior to transfer (for details, see SI). This resulted in sheet rupturing. Typical images are contained in Figure 4d−f, and the height values are collected in Table 1.

Table 1. Thickness *d*, Scattering Length Density SLD, and Root-Mean-Square Roughness *σ* of ML2 and S2$_{400-20'000}$ as Determined by X-ray Reflectivity (XRR) at the Air/Water Interface and Atomic Force Microscopy (AFM) as Well as Neutron Reflectivity (NR) on a Si/SiO$_2$[a] Substrate

	d (Å)	SLD (10^{-6} Å^{-2})	σ (Å)
		XRR[b]	
ML2	17.2 ± 0.1	11.73 ± 0.11	3.1 ± 0.1
S2$_{4000}$	19.6 ± 0.2	12.04 ± 0.06	3.1 ± 0.1
solution		9.45	3 ± 0.1
	d (Å)	SLD (10^{-6} Å^{-2})	σ (Å)[c]
		NR	
ML2	15.3 ± 0.5	2.86 ± 0.04	3
S2$_{400}$	15.7 ± 0.5	3.04 ± 0.04	3
S2$_{4000}$	16.6 ± 0.5	3.51 ± 0.04	3
	d (Å)		
		AFM	
S2$_{400}$	<1		
S2$_{4000}$	19		
S2$_{20'000}$	25		

[a]For the AFM measurements Si/SiO$_2$ (280 nm) was used, and the NR experiments were carried out on a Si wafer with a native oxide layer of ~1 nm. [b]χ2 of the fit remained below 0.03. [c]σ is the rms roughness of the monolayer−air interface.

2.E. Neutron Reflectivity. Specular neutron reflectivity experiments were carried out on time-of-flight reflectometer G3bis in the ORPHEE reactor (Laboratoire Léon Brillouin, CEA-Saclay, France). Each sample was measured at two angles of incidence, $\theta = 0.8$ and 2.5°, using a polychromatic beam with a range of wavelength $\lambda \approx 2.0$ to 25 Å. The vertical slit openings were adjusted so that the angular resolution for both angles of incidence was $\delta\theta/\theta \approx 5\%$. These two configurations give a total range of momentum transfer, $q_z = 4\pi \sin(\theta)/\lambda$, of about 0.007 to 0.27 Å^{-1}. The acquisition times for the reflectivity spectra were 2 h at 0.8° and 15 h at 2.5°.

2.F. X-ray Photoelectron Spectroscopy. XPS is a quantitative surface analysis method. X-rays excite electrons in elements. The kinetic energy of the electrons is linked to the excitation energy and their original binding energy in the element and is thus a fingerprint of that element. Although core electrons mainly feel the Coulomb potential of the nucleus and the neighboring (core-level) electrons, chemical interactions cause small changes in the binding energy of the core levels as well. Thus, the binding energy of XPS electrons also reveals the chemical state of the element. As electrons can travel only a few angstroms in most materials, only electrons from near the surface can leave the materials and are later detected by the electron analyzer. In calibrating the system by considering the transmission factor of the spectrometer, the elementary photoemission yield, and the mean free path, the number of electrons assigned to a certain element allows us to measure element concentration with a detection limit of 0.1 to 1 atom %.[37]

2.G. Rutherford Backscattering. The samples were characterized by Rutherford backscattering spectrometry (RBS)[38] at the ETH Laboratory of Ion Beam Physics. Measurements were performed on monolayers of S2$_{400}$, S2$_{4000}$, and S2$_{20'000}$ on Si/SiO$_2$ using a 2 MeV ^{4}He beam and a silicon PIN diode detector under 168°. The collected RBS data was analyzed using the RUMP code.[39] The area density of Ni atoms at the surface was normalized to the substrate signal height. The small Ni signal is sitting on a flat background caused by event pile-up from the sample substrate. On the one hand, this background has been simulated by the RUMP code. On the other hand, it was removed by the subtraction of a linear background level. Both data

analysis techniques lead to results that agree within statistical uncertainty that amounts to approximately 15%. The systematic uncertainty is around 5% and is mainly caused by the calculation of the substrate signal height. RBS measures a higher Ni ratio than the other techniques. Because all of the samples measured by RBS have also been investigated by AFM, it can be excluded that the sheets were partially folded. RBS has a depth resolution of a few tens of nanometers. The technique can therefore not distinguish between complexed Ni and residual Ni that might be directly below the molecular monolayer or might have diffused into the substrate.

Because this method is not often used in the analysis of organic monolayers, a brief explanation can be found in the Supporting Information.

3. RESULTS

3.A. BAM. After the spreading of monomer **2**, the isotherm was recorded. Figure 3 shows the corresponding surface
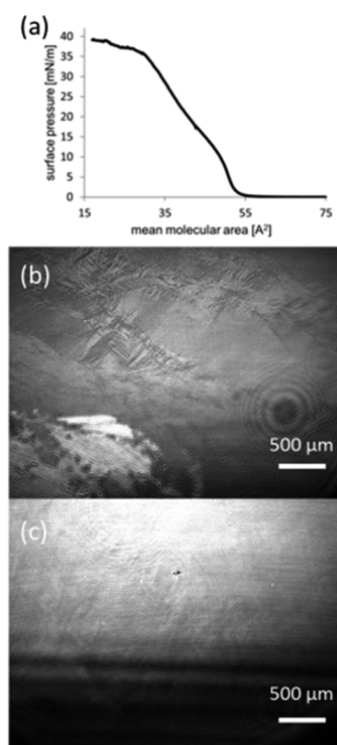

Figure 3. (a−c) Monomer **2** at the air/water interface. (a) Isotherm of monomer **2** used to determine the mean molecular area $A = 52$ Å^2 at an SP of $\pi = 8$ mN/m. BAM images at SP = 8 mN/m before salt injection (b) and 8 h after injection (c). The darker appearance in the lower part of the image is a consequence of water evaporation.

pressure (SP)/mean molecular area (MMA) curves and some BAM images. At pressures higher than approximately 8 mN m^{-1}, the isotherm indicates processes beyond simple monolayer formation until the final collapse pressure of ~32 mN m^{-1} is reached. The MMA for **2** from the well-behaved part of the isotherm at 8 mN/m is 52 Å^2. This value is used throughout for the determination of the Ni^{2+}/**2** ratio. The BAM images, after the typical formation of islands (not shown), indicate irregularities in the ML (Figure 3b). These irregularities remain even after an equilibration period of 13 h. The microscope was moved to a few other sites on the interface where similar images were obtained. Thus, the disorder probably concerns the entire monolayer on the 20 × 50 cm^2-sized trough. Interestingly, virtually independent of the
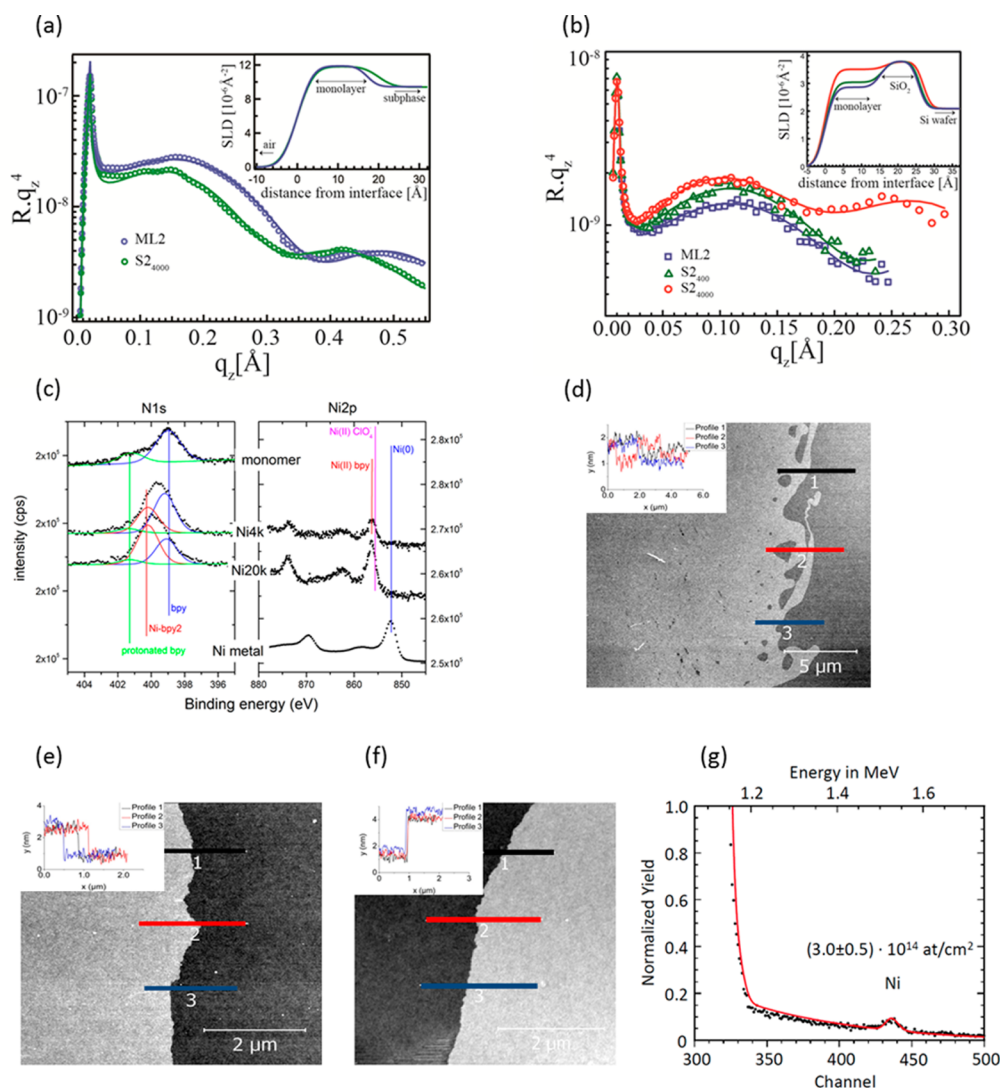
Figure 4. Analysis of $S2_{400}$, $S2_{4000}$, and $S2_{20'000}$ by XRR (a), NR (b), XPS (c), TM-AFM (d−f), and RBS (g) of **ML2** and various $S2_{Ni}$. (a) X-ray reflectivity of monolayers at the air/water interface. Solid lines are best-fit curves: **ML2** (blue circles) and $S2_{4000}$ (green circles). The corresponding sld profiles are shown in the inset. (b) Neutron reflectivity of transferred monolayers on a Si wafer. Solid lines are best-fit curves: **ML2** (blue squares), $S2_{400}$ (green triangles), and $S2_{4000}$ (red circles). The sld profiles are shown in the inset. (c) XP spectra of the N 1s (left) and Ni 2p (right) states for various $S2_{Ni}$. For comparison, the spectra of metallic Ni and monomer **2** are included. The N 1s signal is deconvoluted into contributions from N in bpy, Ni-coordinated bpy, and protonated bpy. The Ni states are solely attributed to Ni(II) coordinated with bpy. (d−f) TM-AFM images taken on Si/SiO$_2$ (280 nm). For height profiles, see insets. (g) RBS of a monolayer sheet. The Ni peak sits on a flat background produced by event pile up from the substrate signal. The solid red line is a simulation representing the best fit of the Ni surface coverage.

applied $Ni^{2+}/2$ ratios, the MLs finally become homogeneous as judged by BAM (Figure 3c). Thus, the presence of the salt has a direct impact on the structure of the monolayer.

3.B. XRR. Figure 4a shows the measured XRR curves of monomer MLs before (green circles) and 7 h after Ni-salt injection (blue circles). The red solid lines represent the best matching fits. The obtained structure parameters corresponding to the best matching fit are summarized in the inset of Figure 4 and Table 1. The thickness of monolayer **ML2** is 17.2 Å. After the injection of Ni salt into the subphase, the thickness of resulting sheet $S2_{4000}$ increases by 2.4 Å to 19.6 Å. Additionally, the thickness increase is combined with a slight increase in the scattering-length density (Figure 4a), indicating the enrichment of ions near the air/water interface. We therefore assign this increase to a binding interaction between the monomers and Ni^{2+}. This increase allows us to estimate the excess number of electrons of $S2_{4000}$ after the addition of Ni^{2+} ions as $N_e =$

$A_m(d_{s2_{4000}} \rho_{S2_{4000}} - d_{ML2}\rho_{ML2})$, where A_m is the area per monomer **2** and d is the sheet thickness. ρ is the electron density related to the scattering-length density as $\rho = SLD/r_e$, where $r_e = 2.818 \times 10^{-15}$ m is the classical radius of the electron. By assuming two perchlorate counterions per one Ni^{2+} ion and using the values in Figure 4a, the number of Ni ions per monomer molecule **2** is derived to be 0.61 ± 0.18 (Table 2).

3.C. NR. For the bare silicon wafer, the reflectivity profile indicates the presence of a native oxide layer of about 10.4 ± 0.5 Å; this oxide layer is taken into account when data fitting the transferred monolayers. Thus, the reflectivity curves are fitted with a two-layer model, with the first layer describing the transferred monolayer and the second describing the oxide layer. The variable parameters are the scattering-length density Nb and thickness d of each layer plus the width of each interface as described by an error function. To optimize the information on the monolayer, the native oxide layer is

Table 2. Determination of the Ni^{2+}/2 Ratio in Sheet S2$_{Ni}$ by XRR at the Air/Water Interface, by NR and RBS on the Si Wafer, and by XPS on Au

method	S2$_{Ni}$	Ni(II)/2
XRR	S2$_{4000}$	0.6 ± 0.2[a,b]
NR	S2$_{400}$	<0.5[a,b]
	S2$_{4000}$	1.1[a,b]
RBS	S2$_{400}$	Ni below detection limit
	S2$_{4000}$	1.7[b]
	S2$_{20000}$	1.8[b]
XPS Ni 2p	S2$_{4000}$	0.6 ± 0.5
	S2$_{20000}$	1.0 ± 0.5

[a]Assuming 2 perchlorate counterions per Ni(II). [b]Assuming MMA = 52 Å^2 as suggested by the isotherm.

assumed to be unchanged. Moreover, the lowest interfacial roughnesses are fixed at 3 Å to complementarily unite the XRR and NR analyses. This enables one to refine the fitting of the scattering-length density Nb and thickness d of the monolayer.

For monolayer **ML2**, the best-fit values to the reflectivity curve (shown in Figure 4b) are $d = 15.3 \pm 0.5$ Å and $Nb = (2.86 \pm 0.04) \times 10^{-6}$ Å^{-2}; for sheet **S2**$_{400}$, $d = 15.7 \pm 0.5$ Å and $Nb = (3.04 \pm 0.04) \times 10^{-6}$ Å^{-2}; and for sheet **S2**$_{4000}$, $d = 16.6 \pm 0.5$ Å and $Nb = (3.51 \pm 0.04) \times 10^{-6}$ Å^{-2}. The significant increase in the scattering-length density after injection with Ni^{2+} indicates the accumulation of Ni^{2+} (and its counterion perchlorate) in the monolayer, with an accompanying small increase in thickness. If this increase in Nb is attributed only to the presence of Ni^{2+} and its counterion ClO$_4^-$, then it is possible to estimate the amount of Ni^{2+} and ClO$_4^-$ from $\phi_{Ni}Nb(Ni) + \phi_{ClO4}Nb(ClO_4^-) = \Delta Nb = 0.18 \times 10^{-6}$ Å^{-2} for **S2**$_{400}$ and 0.65×10^{-6} Å^{-2} for **S2**$_{4000}$. ϕ_N and ϕ_{ClO4} are the volume fractions of the species in the sheet, and $Nb(Ni) = 9.406 \times 10^{-6}$ Å^{-2} and $Nb(ClO_4^-) = 4.00 \times 10^{-6}$ Å^{-2}, the theoretical estimates of their scattering-length densities with corresponding molecular volumes of $\nu_{Ni} = 11$ Å^3 and $\nu_{ClO4} = 82$ Å^3.[40] For the dry transferred layer, it is reasonable to consider the condition of electroneutrality where each Ni^{2+} is associated with two ClO$_4^-$ ions.

From mass balance in the monolayer $\phi_{Ni} + \phi_{ClO4} + \phi_2 = 1$ where ϕ_2 is the volume fraction of monomer **2**, the concentration of each species can be estimated. These results give <0.5 Ni per monomer **2** for **S2**$_{400}$ and ∼1 Ni per monomer **2** for **S2**$_{4000}$ (Table 2).

3.D. XPS. The qualitative analysis of monolayer-thick membranes by XPS is straightforward. Figure 4c shows a series of N 1s and Ni 2p spectra taken from monolayer **ML2** and sheets **S2**$_{4000}$ and **S2**$_{20'000}$ as well as from Ni metal. We focus on the peaks from N 1s and Ni 2p orbitals. We note that the binding energy of the Ni 2p electrons matches that of literature values for Ni. Then we see that the observed binding energy of Ni 2p electrons is clearly different from that of Ni 2p in Ni(ClO$_4$)$_2$, which justifies their assignment as Ni^{2+}(bpy)$_{1,2}$. This is evidence that Ni^{2+} has reacted with monomer **2**. The result is supported by the corresponding changes in the N 1s peaks. Comparing the measured binding energies to those of monomer **2**, the three contributions to the N 1s peak are interpreted as the nitrogen atoms in the bpy's, which are not coordinated to Ni^{2+}, protonated nitrogen atoms, and nitrogen atoms coordinated to Ni^{2+}. The amount of Ni-coordinated bpy increases with the Ni salt concentration applied during polymerization.

A quantitative analysis by XPS requires a structural model because the thickness of the membrane (approximately 1.9 nm) is similar to the excitation length of photoelectrons. Electrons from atoms at the bottom of the membrane contribute differently to the signal than those from the top. In homogeneous samples, this is implemented in the calibration factor (sensitivity factor). However, the structural characterizations of the films by AFM, XRR, and NR as well as by MMA hint at a structure of the polymer in which the monomers are standing more or less upright with two bpy units and their Ni ions at the bottom (pointing toward the water interface). In this case, the Ni intensity is reduced by the factor e$^{-x/\lambda}$, where x is the membrane thickness and λ is the excitation depth of the Ni photoelectrons. With $\lambda = 2$ nm (for Ni 2p electrons in organic matter)[41] and $x = 1.9$ nm, the Ni concentration is thus underestimated by a factor of 2.6. The thus-derived Ni content is 2.2 atom % for **S2**$_{20'000}$, which corresponds to approximately 1 ± 0.5 Ni atoms per monomer **2**. We mention that this number is error prone. On one hand, we have the typical error of 0.5 atom % due to intrinsic measurement uncertainties and data fitting; on the other hand, there is an uncertainty regarding sheet thickness. Furthermore, any other molecules sticking to the surface (water, CO$_2$, residue from the polymerization reaction) will falsify the result. Apart from the absolute amount, the Ni contents clearly show a trend, which is in agreement with the changes in the N 1s indicating a varying nitrogen/nickel interaction: the ratio of noncomplexed bpy to Ni^{2+}-complexed bpy depends on the feed concentration. This aspect has a bearing on the question of whether **S2**$_{Ni}$ sheets have a preferred Ni^{2+}/2 ratio or, in other words, whether they have a defined stoichiometry between their constituents (monomer **2** and Ni^{2+}). It seems that this can be the case only for high Ni^{2+}/2 ratios, if at all.

3.E. AFM. Attempts to measure the **ML2** by AFM on mica and on silicon failed. The edges were created as described (SI), but the features observed were ill-defined, indicating substantial positional freedom of the monomer (Figure S1) and also including the option to lie flat on the solid substrate. Instead, AFM heights were successfully determined for **S2**$_{400}$, **S2**$_{4000}$, and **S2**$_{20'000}$, and Table 1 provides the corresponding height values.

4. DISCUSSION

If one assumes that the monomer lies flat on the interface, then a simple hexagonal structure model based on ChemDraw using disclike objects of the same dimensions as **2** suggests an upper threshold for the MMA of 300 Å^2 (Figure 2). Despite the fact that the BAM images showed the monolayer not to be macroscopically homogeneous, hinting toward a larger-than-observed MMA, the small value of 52 Å^2 suggests that the monomer almost takes an upright orientation. For such a geometry, the same model suggests MMA = 63 Å^2 for monomer **2**, which is in reasonable agreement with the experiment given the uncertainties mentioned.

Next, the thickness of the ML was investigated. The expectation value for a vertical arrangement was $h_{model} \approx 16$ Å (Figure 2). This seems to explain the thickness of an **ML2** monolayer obtained by XRR, $h_{ML2} = 17.2$ Å for **ML2**. Comparing the thickness values obtained for **ML2** and **S2**$_{4000}$ by XRR, a clearly larger **S2**$_{4000}$ thickness ($h_{S2,4000(XRR)} = 19.6$ Å) indicates the binding of **ML2** and Ni^{2+}. The same tendency was observed by NR and AFM (Table 1). This seems to reflect the change in the molecular tilt angle with respect to the direction
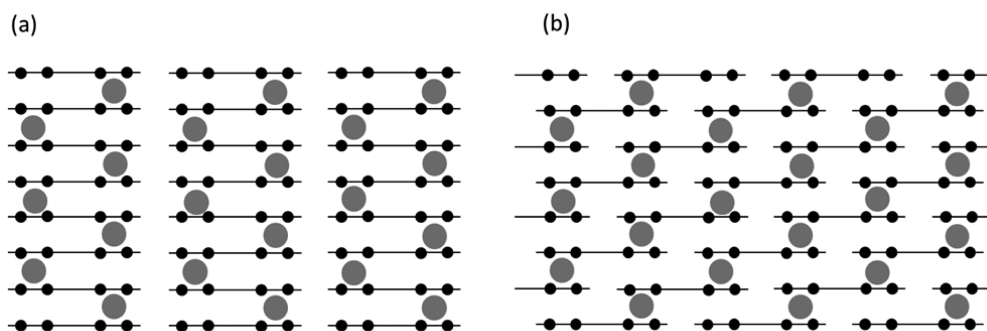
Figure 5. Top view of idealized molecular models (a) and (b) for the complexation between monomer **2** and Ni^{2+}. The monomer is represented as a line with the two bpy's pointing downward, shown as pairs of black dots and disregarding the bpy unit pointing upward, away from the interface. The tilt angle is set to be 90°. The gray spheres represent Ni^{2+}. Linear chains with the director axis perpendicular (a) and tilted to the monomer orientation (b). Both models involve weak complexes that should allow for metal ion exchange processes to occur. This model disregards the actual complexation geometry, which ideally should be square planar.

normal to the surface and the change in water level due to Ni^{2+} binding. Moreover, the fact that the thickness of **S2**$_{4000}$ obtained by AFM ($h_{S2,4000(AFM)} = 19$ Å) is comparable to that on the water surface implies that the transfer of **S2** films to a solid substrates does not alter the molecular orientation drastically. It is noted that the edges of **S2**$_{4000}$ used for the height determination appear to be brittle, which, interestingly, suggests the sheet to be a cohesive entity. It is further noted that the thickness values obtained by NR were slightly lower compared to those obtained from the other techniques (Table 1). This can be attributed to hydrogen atoms that are incoherent scatterers and have a low SLD contrast with air. Therefore, these atoms contribute only to the background level but not to structural information, as reported for other organic thin films.[42−46] When the molar ratio of Ni^{2+} was low (**S2**$_{400}$), AFM suggested fuzzy features near the film periphery, which are reminiscent of fluidlike behavior (Figure 4d). This makes it difficult to determine the film thickness (Table 1), suggesting that the degree of Ni complexation is very poor, if there is any. In fact, there is no sizable effect on the mechanical coherence by clamping monomers together by intermolecular Ni(bpy)$_2$ complexes. Consequently, **S2**$_{400}$ is not a cohesive sheet such as **S2**$_{4000}$. This argumentation is in line with the NR data on **S2**$_{400}$, which show only a very small increase in thickness. According to the increase in the Ni^{2+} molar ratio to **S2**$_{4000}$ (Figure 4e), the film thickness measured by AFM (19 Å) shows very good agreement with those determined by XRR and NR. However, at a high Ni^{2+} molar ratio (**S2**$_{20000}$, Figure 4f), the thickness of the transferred **S2** monolayer obtained by AFM (25 Å) is much greater than what one can imagine from the molecular size, suggesting an artifact from excess salts. Thus, our results convey a clear message that the complexation does not drive a pulling down of the monomers to lie flat on the interface.

In the next step, the incorporation of Ni^{2+} into **S2** sheets was determined. In addition, RBS (Figure 4g) was measured for **S2** sheets prepared at different molar ratios. There it first needs to be clarified that the ratios obtained by XRR, NR, and RBS refer to the ones between the total number of Ni^{2+} and the total number of monomers and thus disregard whether Ni^{2+} is engaged in complexation. The binding stoichiometry values calculated from the experimental data are compiled in Table 2. Despite the technical limit of each technique and various assumptions made (Materials and Methods section), the values in Table 2 are in reasonable agreement, which allows us to draw

the following two conclusions: (i) Ni^{2+} is unequivocally part of all **S2** sheets and (ii) the Ni^{2+}/**2** ratio is on the order of unity.

The RBS and XPS measurements deserve further comment. The RBS values for **S2**$_{4000}$ and **S2**$_{20'000}$ suggest a higher Ni^{2+}/**2** ratio than for the other methods. While we do not yet fully understand where this difference comes from, it is mentioned that the RBS signal is relatively broad and may convolute contributions from Ni or other neighboring elements (in particular Fe) contained in the substrate, resulting in somewhat higher ratios than those measured by the surface-sensitive techniques. This may also explain why the two ratios obtained for the two samples differ only slightly.

The spectral analysis of the XPS N 1s signal (Figure 4c, left panel) allows for the discrimination of N in noncoordinated bpy (blue), protonated N (green), and N coordinated to Ni (red). First, as presented in the figure, the signal from the protonated bpy (green) is close to the baseline. Second, the ratio between Ni-complexed bpy and noncomplexed bpy (bpy$_{Ni}$/bpy) monotonically increases with the feed ratio of Ni^{2+}, reaching ∼2 for **S2**$_{20'000}$. This seems reasonable from the orientation of the monolayer suggested from XRR and NR, where one-third of bipyridine moieties stick out to the air phase and thus cannot form complexes with Ni^{2+}. However, it should be noted that it is not possible to discriminate Ni(bpy)$^{2+}$ vs Ni(bpy)$_2$$^{2+}$.

XPS results are not only in qualitative agreement with the ratio estimates given in Table 2 but also suggest that there is no stable complex between Ni^{2+} and the bpy units of compound **2** in **S2**$_{Ni}$ sheets, which would cause a fixed ratio between these two components representative of an energetic minimum. This aspect needs to be accounted for in a molecular model for sheet **S2** (see below).

The analysis of the Ni 2p signals supports the increasing complexation of the bpy units with increasing Ni^{2+} in the feed. As Figure 4c (right panel) shows, the intensity of the Ni 2p signal due to complex formation increases when going from **S2**$_{4000}$ to **S2**$_{20'000}$. Thus, XPS independently confirms the Ni^{2+}/**2** ratio of unity as given in Table 2, which is consistent with the conclusions drawn from the analysis of the N 1s signals.

Figure 5 schematically represents the lateral assembly of the **S2**$_{20'000}$ sheet (sheet at saturation). It is assumed that each metal center is engaged in [Ni(bpy)$_2$]$^{2+}$ complexes as suggested by the XPS results. It is also considered reasonable to assume that bpy's do not bridge two Ni^{2+}. Consequently, only linear chains of a novel metal−organic polymer can form; networks

are not accessible. The mechanical cohesiveness of the sheet, as indicated by the sharp edges visible in the AFM images (Figures 4e,f), is a result of monomer/monomer contacts and of this complexation. When going to lower ratios, an increasing number of Ni sites remain empty (e.g., approximately one-half for $S2_{4000}$), which in turn increasingly reduces the mechanical integrity of the sheet all the way to $S2_{400}$, where the film edges appear liquidlike (Figure 4d, h_{AFM} in Table 1). Further experiments with grazing incidence X-ray diffraction would help us gain a more precise picture of intermolecular coordination at the interface.[30,31]

5. CONCLUSIONS

Monomer **2** spread at the air/water interface and a Ni^{2+} salt provided in the subphase react with one another. The molecular-scale encounters associated with this were investigated by XRR, NR, RBS, XPS, and AFM both at the interface and after transfer of the different entity formed at the interface onto solid substrates. This study sheds light on what happens to the monomer at the interface before it is exposed to the metal ion. What does the metal ion do to the initial monomer arrangement, and what is the final situation for extreme $Ni^{2+}/2$ ratios for an extreme excess of Ni^{2+}?

The key findings are the following: (a) Compound **2** stands up at the interface and cannot be pulled down to lie flat on the water by complexation irrespective of the $Ni^{2+}/2$ ratio applied to the system. (b) The $Ni^{2+}/2$ ratio in $S2_{4000}$ is approximately unity, although XPS gives a somewhat smaller value and RBS gives a somewhat larger value. (c) $S2_{400}$ is not a good sheet. Not only are its thickness and the $Ni^{2+}/2$ ratio too low but also AFM shows liquidlike edges, suggesting mobility within the sheet. (d) $S2_{4000}$ appears to be a good yet not perfect sheet. The thickness values from XRR and AFM agree well with the expected ones assuming an upright orientation. The NR thickness value is somewhat lower but still in an acceptable range. The $Ni^{2+}/2$ ratio of this sheet from NR is 1.1, which supports the molecular model proposed in Figure 5; however, we note that this method as well as XRR does not allow us to differentiate between Ni ions that are complexed to the bpy units of compound **2** and those that are not. The corresponding ratio from XPS and XRR is lower (0.6), which, particularly in regard to the XPS result, may suggest that not all Ni positions in this model are occupied. (e) $S2_{20'000}$ was investigated by XPS mainly with the intention to determine whether the nickel complexation can be pushed to the required $Ni^{2+}/2$ ratio of unity. This in fact was found to further support the model in Figure 5. (f) There is no defined chemical entity of monomer **2** and Ni^{2+} to which a fixed stoichiometry could be assigned that would represent a sizable energy minimum. Rather, the seemingly stoichiometric situation in $S2_{20'000}$ in which all of the bpy units pointing toward the interface are actually engaged in complex formation is enforced by the huge excess of Ni^{2+} to monomer.

We present two related molecular models accounting for this. They invoke metal–organic chain polymers that also explain part of the increasing mechanical coherence with the $Ni^{2+}/2$ ratio. While we have failed the initial goal to use monomer **2** for the creation of 2D networks, the present work shows a simple method of how to create mechanically coherent sheets between monomer **2** and Ni^{2+} (in particular for $S2_{4000}$). These sheets suggest stunning opportunities resulting from (i) the weakness of the complexes involved and (ii) the molecular model suggesting an unused bpy unit (a spectator) that each

monomer presents on the side of the sheet opposite to the Ni complexes. Because the complexes that undoubtedly form between the bpy units and Ni^{2+} do not represent a strong, persistent complex, the sheets may be used to exchange some of the Ni^{2+} ions by other transition-metal ions resulting in a dense array of different metal ions held together in a sheet. Such a scenario could be of interest in catalysis.[47] The other opportunity is to use the unused bpy units for the complexation of a different metal ion resulting in a nanosheet, the two sides of which carry rather dense arrays of (at least) two different metals, which appear to be an unprecedented array. Finally, we note that the sheets described here expand the range of supramolecular sheets reported by various groups.[48−53]

■ ASSOCIATED CONTENT

Ⓢ Supporting Information

The Supporting Information is available free of charge on the ACS Publications website at DOI: 10.1021/acs.langmuir.6b04282.

> Materials and Methods, synthesis of monomer **2**, NMR spectra of monomer **2**, AFM image of **ML2** after transfer onto Si/SiO$_2$ (280 nm) (PDF)

■ AUTHOR INFORMATION

ORCID Ⓘ
Motomu Tanaka: 0000-0003-3663-9554
A. Dieter Schlüter: 0000-0001-9975-9831

Present Address
(Z.Z.) Department of Chemistry and Food Chemistry, Technical University Dresden, Mommsenstr. 4, 01069 Dresden, Germany.

Notes
The authors declare no competing financial interest.

■ ACKNOWLEDGMENTS

■ REFERENCES

(1) Gee, G.; Rideal, E. K. Reactions in Monolayers of Drying Oils. The Oxidation of the Maleic Anhydride Compound of β-Elaeostearin. *Proc. R. Soc. London, Ser. A* **1935**, *153*, 116−128.

(2) Gee, G. 156. Catalysed polymerisation in monolayers of drying oils. *J. Chem. Soc.* **1937**, 772−778.

(3) Payamyar, P.; King, B. T.; Öttinger, H. C.; Schlüter, A. D. Two-dimensional polymers: concepts and perspectives. *Chem. Commun.* **2016**, *52*, 18−34.

(4) Sakamoto, J.; van Heijst, J.; Lukin, O.; Schlüter, A. D. Two-Dimensional Polymers: Just a Dream of Synthetic Chemists? *Angew. Chem., Int. Ed.* **2009**, *48*, 1030−1069.

(5) Colson, J. W.; Dichtel, W. R. Rationally synthesized two-dimensional polymers. *Nat. Chem.* **2013**, *5*, 453−465.

(6) Zhuang, X.; Mai, Y.; Wu, D.; Zhang, F.; Feng, X. Two-Dimensional Soft Nanomaterials: A Fascinating World of Materials. *Adv. Mater.* **2015**, *27*, 403−427.

(7) Lackinger, M. On-surface polymerization − a versatile synthetic route to two-dimensional polymers. *Polym. Int.* **2015**, *64*, 1073−1078.

(8) Zang, Y.; Aoki, T.; Teraguchi, M.; Kaneko, T.; Ma, L.; Jia, H. Two-Dimensional and Related Polymers: Concepts, Synthesis, and their Potential Application as Separation Membrane Materials. *Polym. Rev.* **2015**, *55*, 57−89.

(9) Baek, K.; Hwang, I.; Roy, I.; Shetty, D.; Kim, K. Self-Assembly of Nanostructured Materials through Irreversible Covalent Bond Formation. *Acc. Chem. Res.* **2015**, *48*, 2221−2229.

(10) Boott, C. E.; Nazemi, A.; Manners, I. Synthetic Covalent and Non-Covalent 2D Materials. *Angew. Chem., Int. Ed.* **2015**, *54*, 13876− 13894.

(11) Kissel, P.; Erni, R.; Schweizer, W. B.; Rossell, M. D.; King, B. T.; Bauer, T.; Götzinger, S.; Schlüter, A. D.; Sakamoto, J. A two-dimensional polymer prepared by organic synthesis. *Nat. Chem.* **2012**, *4*, 287−291.

(12) Kory, M. J.; Wörle, M.; Weber, T.; Payamyar, P.; van de Poll, S. W.; Trapp, N.; Schlüter, A. D. Gram-scale synthesis of two-dimensional polymer crystals and their structure analysis by X-ray diffraction. *Nat. Chem.* **2014**, *6*, 779−784.

(13) Kissel, P.; Murray, D. J.; Wulftange, W. J.; Catalano, V. J.; King, B. T. A nanoporous two-dimensional polymer by single-crystal-to-single-crystal photopolymerization. *Nat. Chem.* **2014**, *6*, 774−778.

(14) Bhola, R.; Payamyar, P.; Murray, D. J.; Kumar, B.; Teator, A. J.; Schmidt, M. U.; Hammer, S. M.; Saha, A.; Sakamoto, J.; Schlüter, A. D.; King, B. T. A Two-Dimensional Polymer from the Anthracene Dimer and Triptycene Motifs. *J. Am. Chem. Soc.* **2013**, *135*, 14134− 14141.

(15) Bauer, T.; Zheng, Z.; Renn, A.; Enning, R.; Stemmer, A.; Sakamoto, J.; Schlüter, A. D. Synthesis of Free-Standing, Monolayered Organometallic Sheets at the Air/Water Interface. *Angew. Chem., Int. Ed.* **2011**, *50*, 7879−7884.

(16) Zheng, Z.; Ruiz-Vargas, C. S.; Bauer, T.; Rossi, A.; Payamyar, P.; Schütz, A.; Stemmer, A.; Sakamoto, J.; Schlüter, A. D. Square-Micrometer-Sized, Free-Standing Organometallic Sheets and Their Square-Centimeter-Sized Multilayers on Solid Substrates. *Macromol. Rapid Commun.* **2013**, *34*, 1670−1680.

(17) Payamyar, P.; Kaja, K.; Ruiz-Vargas, C.; Stemmer, A.; Murray, D. J.; Johnson, C. J.; King, B. T.; Schiffmann, F.; Vandevondele, J.; Renn, A.; Götzinger, S.; Ceroni, P.; Schütz, A.; Lee, L. T.; Zheng, Z.; Sakamoto, J.; Schlüter, A. D. Synthesis of a Covalent Monolayer Sheet by Photochemical Anthracene Dimerization at the Air/Water Interface and its Mechanical Characterization by AFM Indentation. *Adv. Mater.* **2014**, *26*, 2052−2058.

(18) Murray, D. J.; Patterson, D. D.; Payamyar, P.; Bhola, R.; Song, W.; Lackinger, M.; Schlüter, A. D.; King, B. T. Large Area Synthesis of a Nanoporous Two-Dimensional Polymer at the Air/Water Interface. *J. Am. Chem. Soc.* **2015**, *137*, 3450−3453.

(19) Sakamoto, R.; Hoshiko, K.; Liu, Q.; Yagi, T.; Nagayama, T.; Kusaka, S.; Tsuchiya, M.; Kitagawa, Y.; Wong, W.-Y.; Nishihara, H. A photofunctional bottom-up bis(dipyrrinato)zinc(II) complex nanosheet. *Nat. Commun.* **2015**, *6*, 6713−6718.

(20) Takada, K.; Sakamoto, R.; Yi, S.-T.; Katagiri, S.; Kambe, T.; Nishihara, H. Electrochromic Bis(terpyridine)metal Complex Nanosheets. *J. Am. Chem. Soc.* **2015**, *137*, 4681−4689.

(21) Baek, K.; Yun, G.; Kim, Y.; Kim, D.; Hota, R.; Hwang, I.; Xu, D.; Ko, Y. H.; Gu, G. H.; Suh, J. H.; Park, C. G.; Sung, B. J.; Kim, K. Free-Standing, Single-Monomer-Thick Two-Dimensional Polymers through Covalent Self-Assembly in Solution. *J. Am. Chem. Soc.* **2013**, *135*, 6523−6528.

(22) Zhang, K.-D.; Tian, J.; Hanif, D.; Zhang, Y.; Sue, A. C.-H.; Zhou, T.-Y.; Zhang, L.; Zhao, X.; Liu, Y.; Li, Z.-T. Toward a Single-Layer Two-Dimensional Honeycomb Supramolecular Organic Framework in Water. *J. Am. Chem. Soc.* **2013**, *135*, 17913−17918.

(23) Makrlík, E.; Vaňura, P. Stability constants of tris(2,2′-bipyridine) complexes of Fe²⁺, Co²⁺, Ni²⁺, Cu²⁺ and Zn²⁺ in 1,2-dichloroethane saturated with water. *Colloids Surf.* **1992**, *68*, 195−197.

(24) Vander Griend, D. A.; Bediako, D. K.; DeVries, M. J.; DeJong, N. A.; Heeringa, L. P. Detailed Spectroscopic, Thermodynamic, and Kinetic Characterization of Nickel(II) Complexes with 2,2′-Bipyridine

(25) Ruaudel-Teixier, A.; Barraud, A.; Belbeoch, B.; Roulliay, M. Langmuir-Blodgett films of pure porphyrins. *Thin Solid Films* **1983**, *99*, 33−40.

(26) Möhwald, H.; Miller, A.; Stich, W.; Knoll, W.; Ruaudel-Teixier, A.; Lehmann, T.; Fuhrhop, J.-H. Intermolecular interactions in monolayers of porphyrins. *Thin Solid Films* **1986**, *141*, 261−275.

(27) Chou, H.; Chen, C.-T.; Stork, K. F.; Bohn, P. W.; Suslick, K. S. Langmuir-Blodgett Films of Amphiphilic Push-Pull Porphyrins. *J. Phys. Chem.* **1994**, *98*, 383−385.

(28) Fouriaux, S.; Armand, F.; Araspin, O.; Ruaudel-Teixier, A.; Maya, E. M.; Vazquez, P.; Torres, T. Effect of the Metal on the Organization of Tetraamidometallophthalocyanines in Langmuir− Blodgett Films. *J. Phys. Chem.* **1996**, *100*, 16984−16988.

(29) Liu, H.-G.; Feng, X.-S.; Xue, Q.-B.; Wang, L.; Yang, K.-Z. Central metal effect on the organization of porphyrin LB films. *Thin Solid Films* **1999**, *340*, 265−270.

(30) Makiura, R.; Konovalov, O. Interfacial growth of large-area single-layer metal-organic framework nanosheets. *Sci. Rep.* **2013**, *3*, 2506.

(31) Makiura, R.; Konovalov, O. Bottom-up assembly of ultrathin sub-micron size metal−organic framework sheets. *Dalton Trans.* **2013**, *42*, 15931−15936.

(32) Soliman, A. M.; Fortin, D.; Harvey, P. D.; Zysman-Colman, E. Hybrid charged heterometallic Pt−Ir complexes: tailoring excited states by taking the best of both worlds. *Chem. Commun.* **2012**, *48*, 1120−1122.

(33) Kiehne, U.; Bunzen, J.; Staats, H.; Lutzen, A. Synthesis of Substituted 2,2′-Bipyridines from 2-Bromo- or 2-Chloropyridines Using Tetrakis(triphenylphosphine)palladium(0) as a Catalyst in a Modified Negishi Cross-Coupling Reaction. *Synthesis* **2007**, *2007*, 1061−1069.

(34) Bao, B. Q.; Yuwen, L.; Zhan, X. W.; Wang, L. H. Water-soluble hyperbranched polyelectrolytes with high fluorescence quantum yield: Facile synthesis and selective chemosensor for Hg²⁺ and Cu²⁺ ions. *J. Polym. Sci., Part A: Polym. Chem.* **2010**, *48*, 3431−3439.

(35) Parratt, L. G. Surface Studies of Solids by Total Reflection of X-Rays. *Phys. Rev.* **1954**, *95*, 359−369.

(36) Nelson, A. Co-refinement of multiple-contrast neutron/X-ray reflectivity data using MOTOFIT. *J. Appl. Crystallogr.* **2006**, *39*, 273− 276.

(37) Briggs, D., Seah, M. P., Eds.; *Practical Surface Analysis - Auger and X-ray Photoelectron Spectroscopy*, 2nd ed.; Wiley Interscience, 1990.

(38) Wang, Y.; Nastasi, M., Eds.; *Handbook of Modern Ion Beam Materials Analysis*; Materials Research Society: Pittsburgh, PA, 2009.

(39) Doolittle, L. R. A semiautomatic algorithm for rutherford backscattering analysis. *Nucl. Instrum. Methods Phys. Res., Sect. B* **1986**, *15*, 227−231.

(40) Jenkins, H. B. D.; Roobottom, H. K.; Passmore, J.; Glasser, L. Relationships among Ionic Lattice Energies, Molecular (Formula Unit) Volumes, and Thermochemical Radii. *Inorg. Chem.* **1999**, *38*, 3609−3620.

(41) Tanuma, S.; Powell, D. J.; Penn, D. R. Calculations of electron inelastic mean free paths. V. Data for 14 organic compounds over the 50−2000 eV range. *Surf. Interface Anal.* **1994**, *21*, 165−176.

(42) Penfold, J.; Thomas, R. K. The application of the specular reflection of neutrons to the study of surfaces and interfaces. *J. Phys.: Condens. Matter* **1990**, *2*, 1369−1412.

(43) Lu, J. R.; Thomas, R. K. Problems in the analysis and interpretation of neutron reflection data. *Nucl. Instrum. Methods Phys. Res., Sect. A* **1995**, *354*, 149−163.

(44) Lee, L.-T.; Jean, B.; Menelle, A. Effect of Temperature on the Adsorption of Poly(N-isopropylacrylamide) at the Air−Solution Interface. *Langmuir* **1999**, *15*, 3267−3272.

(45) Jean, B.; Lee, L.-T.; Cabane, B. Effects of Sodium Dodecyl Sulfate on the Adsorption of Poly(N-isopropylacrylamide) at the Air− Water Interface. *Langmuir* **1999**, *15*, 7585−7590.

(46) Rossetti, F. F.; Schneck, E.; Fragneto, G.; Konovalov, O. V.; Tanaka, M. Generic Role of Polymer Supports in the Fine Adjustment of Interfacial Interactions between Solid Substrates and Model Cell Membranes. *Langmuir* **2015**, *31*, 4473−4480.

(47) Bachmann, C.; Probst, B.; Oberholzer, M.; Fox, T.; Alberto, R. Photocatalytic proton reduction with ruthenium and cobalt complexes immobilized on fumed reversed-phase silica. *Chem. Sci.* **2016**, *7*, 436−445.

(48) Roy, R. K.; Gowd, E. B.; Ramakrishnan, S. Periodically Grafted Amphiphilic Copolymers: Nonionic Analogues of Ionenes. *Macromolecules* **2012**, *45*, 3063−3069.

(49) Aida, T.; Meijer, E.; Stupp, S. I. Functional Supramolecular Polymers. *Science* **2012**, *335*, 813−817.

(50) Sanii, B.; Kudirka, R.; Cho, A.; Venkateswaran, N.; Olivier, G. K.; Olson, A. M.; Tran, H.; Harada, R.; Tan, L.; Zuckermann, R. N.; Shaken. Not Stirred: Collapsing a Peptoid Monolayer To Produce Free-Floating, Stable Nanosheets. *J. Am. Chem. Soc.* **2011**, *133*, 20808−20815.

(51) Liu, K.; Kang, Y.; Wang, Z.; Zhang, X. 25th Anniversary Article: Reversible and Adaptive Functional Supramolecular Materials: "Noncovalent Interaction" Matters. *Adv. Mater.* **2013**, *25*, 5530−5548.

(52) Stupp, S. I.; Palmer, L. C. Supramolecular Chemistry and Self-Assembly in Organic Materials Design. *Chem. Mater.* **2014**, *26*, 507−518.

(53) Vybornyi, M.; Rudnev, A.; Häner, R. Assembly of Extra-Large Nanosheets by Supramolecular Polymerization of Amphiphilic Pyrene Oligomers in Aqueous Solution. *Chem. Mater.* **2015**, *27*, 1426−1431.